PERGAMON

International Journal of Heat and Mass Transfer 43 (2000) 1735–1748

International Journal of HEAT and MASS TRANSFER

www.elsevier.com/locate/ijhmt

On the local thermal equilibrium in microchannel heat sinks

S.J. Kim[a,*], D. Kim[a], D.Y. Lee[b]

[a]Department of Mechanical Engineering, Korea Advanced Institute of Science and Technology, Taejon 305-701, South Korea
[b]Air Conditioning and Environmental Control Laboratory, Korea Institute of Science and Technology, Seoul 130-650, South Korea

Received 2 February 1999; received in revised form 11 August 1999

Abstract

In this paper, analytical solutions for temperature distributions in the microchannel heat sink are obtained by using both one-equation and two-equation models for heat transfer. From the analytical solutions, variables of engineering importance are identified as the Darcy number and the effective thermal conductivity ratio, and their effects are studied. To check the validity of the local thermal equilibrium assumption and the corresponding one-equation model, the relative temperature difference between the fluid and solid phases and the relative error for using the one-equation model are defined. The asymptotic behavior of the relative temperature difference between the phases is examined by using the order of magnitude analysis to confirm the applicability of the local thermal equilibrium assumption and the one-equation model. Finally, the relative error map is presented with respect to variables of engineering importance to identify the applicable region of the one-equation model in practical problems involving the microchannel heat sinks. © 2000 Elsevier Science Ltd. All rights reserved.

Keywords: Local thermal equilibrium; Microchannel heat sink; Porous media

1. Introduction

Microchannel heat sinks have received much attention due to their potential for cooling high-power microelectronic devices. Tuckerman and Pease [1,2] demonstrated that the water-cooled microchannel heat sink is capable of dissipating heat flux of 790 W/cm^2 without a phase change. The high thermal performance of the microchannel heat sink is based on the idea that the heat transfer coefficient is inversely proportional to the hydraulic diameter of the channel. In view of the small dimensions of channels and fins, Koh and Colony [3] noticed that characteristics of fluid flow and heat transfer in the microstructures described in [1,2] are similar to those in porous material. They modeled the microstructures as a porous medium using Darcy's law to describe the flow. Later, Tien and Kuo [4] proposed a model using the Brinkman-extended Darcy equation which accounts for the boundary effect on convection problems. Recently, Kim and Kim [5] reported analytical solutions for velocity and temperature distributions in microchannel heat sinks by modeling the microchannel heat sink as a fluid-saturated porous medium. Their analytical solutions are shown to be in agreement with the closed-form solution for the velocity distribution and the numerical solutions for the conjugate heat transfer problem, which comprises the solid fin and the fluid in the microchannel heat sink. In these studies [3–5], they

* Corresponding author. Tel.: +82-42-869-3043; fax: +82-42-869-3210.
E-mail address: sungkim@me.kaist.ac.kr (S.J. Kim).

PII: S0017-9310(99)00259-8

Nomenclature

a	wetted area per volume
c_f	heat capacity of fluid
C	effective thermal conductivity ratio, $\frac{\varepsilon k_f}{(1-\varepsilon)k_s}$
d_h	hydraulic diameter of the microchannel
D	equivalent Biot number, $\frac{h_l a H^2}{(1-\varepsilon)k_s}$
Da	Darcy number, $\frac{K}{\varepsilon H^2} = \frac{w_c^2}{12H^2}$
E_{1EQ}	relative error for using the one-equation model, $\frac{\theta_f-\theta}{\theta_f}$
E_{LTE}	$\frac{\theta_f-\theta_s}{\theta}$
h_m	heat transfer coefficient based on the bulk-mean temperature
h_l	heat transfer coefficient based on the local temperature
H	channel height
k_f	conductivity of fluid
k_{fe}	effective conductivity of fluid
k_s	conductivity of solid
k_{se}	effective conductivity of solid
K	permeability
L	length of heat sink
$Nu_{\infty,0}$	overall Nusselt number for the fully-developed flow in the microchannel, $\frac{h_m H}{\varepsilon k_f}$
$Nu_{\infty,l}$	local Nusselt number for the fully-developed flow in the microchannel, $\frac{h_l d_h}{k_f}$
p	pressure
P	dimensionless pressure, $\frac{K}{\varepsilon\mu_f u_m}\frac{d\langle p\rangle_f}{dx}$
q_w	heat flux over the bottom surface
T	temperature
T_b	bulk-mean temperature of the fluid
u	velocity
u_m	mean velocity in the fluid region
U	dimensionless velocity, $\frac{\langle u\rangle_f}{u_m}$
w_c	channel width
Y	dimensionless vertical coordinate, $\frac{y}{H}$

Greek symbols

α_s	aspect ratio of the microchannel, $\frac{H}{w_c}$
ε	porosity
ρ_f	density of fluid
θ	dimensionless temperature under local thermal equilibrium, $\frac{\langle T\rangle_f-T_w}{\frac{q_w H}{(1-\varepsilon)k_s}}$
θ_f	dimensionless temperature of fluid, $\frac{\langle T\rangle_f-T_w}{\frac{q_w H}{(1-\varepsilon)k_s}}$
θ_s	dimensionless temperature of solid, $\frac{\langle T\rangle_s-T_w}{\frac{q_w H}{(1-\varepsilon)k_s}}$
μ_f	viscosity of fluid
$\langle\ \rangle_f$	volume-averaged value over the fluid region
$\langle\ \rangle_s$	volume-averaged value over the solid region
$\langle\ \rangle$	volume-averaged value over a REV containing both the fluid and solid phases

used the two-equation model for heat transfer, which treats the fluid and the solid regions separately.

What makes the two-equation model more difficult to apply is the fact that it requires information on the effective conductivity values for the individual phases and the interstitial heat transfer coefficient, which are usually determined through experimental investigations. Even though experimental data are available for heat transfer in packed beds, the interstitial heat transfer coefficient is not generally known a priori for other types of porous media. Moreover, the effective conductivity values depend on the microscopic structure of the porous medium as well as the pure substances comprising the porous medium. Due to these difficulties, many investigators have used the so-called one-equation model for analyses of convection heat transfer in channels filled with porous media. These include Kaviany [6], Vafai and Kim [7], and Poulikakos and Renken [8], to name a few. In the one-equation model, one energy equation covers both the fluid and solid phases, and this simplicity has made the one-equation model a convenient tool for analyzing heat transfer through porous media. However, the one-equation model is valid only when the thermal interaction between the fluid and solid phases is highly effective. In this case, the local temperature difference between them is negligibly small, i.e., the fluid phase is in local thermal equilibrium (LTE hereafter) with the solid phase.

Much research has been conducted to determine the applicable region of the one-equation model for convection through porous media. Carbonell and Whitaker [9] presented the criteria for the validity of LTE approximation based on the order of magnitude analysis. Amiri and Vafai [10] compared the local temperature distributions of the fluid and solid phases by using the numerical solution in the case of flow through a channel filled with a packed bed. They presented an error contour map in terms of the particle Reynolds number and the Darcy number. Recently, Lee and Vafai [11] proposed a criterion for the validity of the one-equation model in the case of flow through a porous channel subject to a constant heat flux on the top and bottom walls by using analytical solutions based on the Darcian flow model for fluid flow and the two-equation model for heat transfer. They focus only on the qualitative presentation of the heat transfer in porous media by taking the effective conductivities and the interstitial heat transfer coefficient as parameters without referring to a specific structure of the porous medium. Even though their work was successful in revealing the general features of the convective heat transfer in porous media, the effect of microscopic structures of the porous medium on the thermal interaction between the solid matrix and the fluid was not covered.

In the present study, a more direct description on the relation between the microscopic structure of the porous medium and the macroscopic convective heat transfer in the porous medium is presented. For this purpose, the heat transfer in a microchannel heat sink, which is a well-organized porous medium, is analyzed theoretically. The microchannel heat sink is attractive in that the interstitial heat transfer coefficient can be determined by the use of numerical experimentation as shown in [4,5]. The main purpose of the present paper is to present a criterion in terms of the parameters concerning the microstructure of the porous media by which we can determine the validity of the LTE and the corresponding one-equation model. To check the validity of the LTE assumption and the corresponding one-equation model, the relative temperature difference between the solid and fluid phases and the relative error for using the one-equation model are defined. The asymptotic behavior of the relative temperature difference between the phases is examined by using the order of magnitude analysis to confirm the applicability of the LTE and the one-equation model to convection heat transfer in the microchannel heat sink. Finally, the relative error map, with respect to the variables of engineering importance, is presented to identify the applicable region of the one-equation model in practical problems involving the microchannel heat sinks.

2. Problem description

The problem under consideration in this paper is forced convective flow through a microchannel as shown in Fig. 1(a). The direction of fluid flow is parallel to x. The bottom surface is uniformly heated and the top surface is insulated. A coolant passes through the microchannel and takes heat away from a heat dissipating component attached to the microchannel heat sink. In analyzing the problem, the flow is assumed to be laminar and both hydrodynamically and thermally fully developed. All thermo-physical properties are assumed to be constant.

The microchannel heat sink is modeled as a porous structure (Fig. 1(b)), as proposed by Tien and Kuo [4].

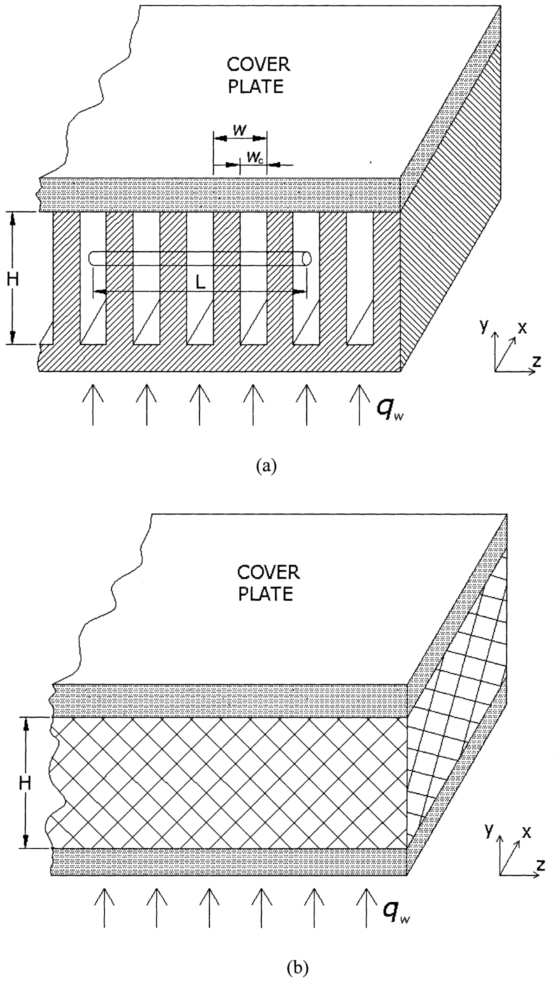

Fig. 1. Porous medium approach: (a) microchannel heat sink; (b) equivalent porous medium.

The governing equations for the velocity and temperature fields in the microstructure are established by applying the volume-averaging technique. The Brinkman-extended Darcy equation, which is developed for describing fluid flow in a porous medium, is used in place of the Darcy equation in order to account for the boundary effect. In obtaining the volume-averaged energy equation, there are two approaches. One is averaging over a representative elementary volume (REV hereafter) containing both the fluid and solid phases, and the other is applying the volume-averaging technique to the solid region and the fluid region separately within the REV. These two models are referred to as the one-equation model and the two-equation model, respectively. Both of them are used to check the validity of the one-equation model against the two-equation model. In the present paper, the REV for volume-averaging is a slender cylinder aligned parallel to the top and bottom walls but perpendicular to the flow direction, as shown in Fig. 1(a). The resultant volume-averaged equations are valid because the REV is long enough to yield statistically meaningful averages, and the direction of volume-averaging is independent of the paths of fluid flow and heat transfer, as pointed out by Kim and Kim [5].

3. Mathematical formulation and solutions

To analyze fluid flow and heat transfer through the microchannel heat sink, the Brinkman-extended Darcy equation and volume-averaged energy equations for the solid and fluid phases are solved.

3.1. Velocity distribution

For the present problem, the Brinkman-extended Darcy equation and boundary conditions are as proposed by Vafai and Tien [12]

$$-\frac{\mathrm{d}}{\mathrm{d}x}\langle p\rangle_\mathrm{f}+\mu_\mathrm{f}\frac{\mathrm{d}^2}{\mathrm{d}y^2}\langle u\rangle_\mathrm{f}-\frac{\mu_\mathrm{f}}{K}\varepsilon\langle u\rangle_\mathrm{f}=0 \tag{1}$$

$$\langle u\rangle_\mathrm{f}=0 \quad \text{at } y=0,H \tag{2}$$

where $\langle\ \rangle_\mathrm{f}$ denotes a volume-averaged value over the fluid region and p, μ_f, u, ε, K and H are pressure, viscosity, velocity, porosity, permeability and channel height, respectively.

For the rectangular microchannel, the porosity and the permeability can be represented as [13]

$$\varepsilon=\frac{w_\mathrm{c}}{w},\qquad K=\frac{\varepsilon w_\mathrm{c}^2}{12}, \tag{3}$$

where w_c and w are channel width and width of fin and channel combined, respectively.

Eq. (1) and boundary condition (BC) (2) can be nondimensionalized by using the following dimensionless variables,

$$U=\frac{\langle u\rangle_\mathrm{f}}{u_\mathrm{m}},\quad Da=\frac{K}{\varepsilon H^2}=\frac{1}{12\alpha_\mathrm{s}^2},\quad Y=\frac{y}{H},\quad P=\frac{K}{\varepsilon\mu_\mathrm{f}u_\mathrm{m}}\frac{\mathrm{d}\langle p\rangle_\mathrm{f}}{\mathrm{d}x}, \tag{4}$$

where u_m is the mean velocity in the fluid region. Note that the Darcy number is inversely proportional to the aspect ratio squared.

Then the dimensionless momentum equation and boundary conditions are expressed as follows;

$$U=Da\frac{\mathrm{d}^2U}{\mathrm{d}y^2}-P \tag{5}$$

$$U=0 \quad \text{at } Y=0,1 \tag{6}$$

When Eq. (5) is solved with BC (6), the velocity distribution is obtained as follows [5]:

$$U=P\left\{\cosh\left(\sqrt{\frac{1}{Da}}Y\right)+\frac{1-\cosh\left(\sqrt{\frac{1}{Da}}\right)}{\sinh\left(\sqrt{\frac{1}{Da}}\right)}\sinh\left(\sqrt{\frac{1}{Da}}Y\right)-1\right\} \tag{7}$$

Since $\int_0^1 U\,\mathrm{d}Y=1$,

$$P=\frac{\sinh\left(\sqrt{\frac{1}{Da}}\right)}{2\sqrt{Da}\left\{\cosh\left(\sqrt{\frac{1}{Da}}\right)-1\right\}-\sinh\left(\sqrt{\frac{1}{Da}}\right)} \tag{8}$$

3.2. Two-equation model

The volume-averaged energy equations and boundary conditions for the solid and fluid phases without the assumption of LTE are expressed as [4,5]

$$k_\mathrm{se}\frac{\partial^2\langle T\rangle_\mathrm{s}}{\partial y^2}=h_\mathrm{l}a(\langle T\rangle_\mathrm{s}-\langle T\rangle_\mathrm{f}) \tag{9}$$

$$\varepsilon\rho_\mathrm{f}c_\mathrm{f}\langle u\rangle_\mathrm{f}\frac{\partial\langle T\rangle_\mathrm{f}}{\partial x}=h_\mathrm{l}a(\langle T\rangle_\mathrm{s}-\langle T\rangle_\mathrm{f})+k_\mathrm{fe}\frac{\partial^2\langle T\rangle_\mathrm{f}}{\partial y^2} \tag{10}$$

$$\langle T\rangle_\mathrm{s}=\langle T\rangle_\mathrm{f}=T_\mathrm{w} \quad \text{at } y=0 \tag{11}$$

$$\frac{\partial\langle T\rangle_\mathrm{s}}{\partial y}=\frac{\partial\langle T\rangle_\mathrm{f}}{\partial y}=0 \quad \text{at } y=H \tag{12}$$

where $\langle\ \rangle_\mathrm{s}$ means a volume-averaged value over the solid region and k_se, T, h_l, a, ρ_f, c_f and k_fe are effective conductivity of the solid matrix, temperature, local heat transfer coefficient, wetted area per volume, density, heat capacity and effective conductivity of fluid, respectively. The local heat transfer coefficient h_l is the proportionality constant between the interfacial heat flux and the solid–fluid temperature difference within the REV.

For the microchannel, the effective conductivities can be represented as [4,5]

$$k_{se} = (1-\varepsilon)k_s, \qquad k_{fe} = \varepsilon k_f, \tag{13}$$

where k_s and k_f are conductivity of solid and conductivity of fluid, respectively.

Eqs. (9)–(12) can be nondimensionalized by using the dimensionless variables listed in Eq. (4) and the following variables,

$$\theta_s = \frac{\langle T\rangle_s - T_w}{\dfrac{q_w H}{(1-\varepsilon)k_s}}, \qquad \theta_f = \frac{\langle T\rangle_f - T_w}{\dfrac{q_w H}{(1-\varepsilon)k_s}} \tag{14}$$

where q_w is the heat flux over the bottom surface of the microchannel heat sink.

For the fully developed flow subject to a constant heat flux, dimensionless equations and boundary conditions are expressed as follows;

$$\frac{d^2\theta_s}{dY^2} = D(\theta_s - \theta_f) \tag{15}$$

$$U = D(\theta_s - \theta_f) + C\frac{d^2\theta_f}{dY^2} \tag{16}$$

$$\theta_s = \theta_f = 0 \quad \text{at } Y = 0 \tag{17}$$

$$\frac{d\theta_s}{dY} = \frac{d\theta_f}{dY} = 0 \quad \text{at } Y = 1, \tag{18}$$

where

$$C = \frac{\varepsilon k_f}{(1-\varepsilon)k_s} \quad \text{and} \quad D = \frac{h_l a H^2}{(1-\varepsilon)k_s}$$

With the velocity distribution given by Eq. (7), energy equations (15) and (16) with BCs (17) and (18) can be solved as follows [5]:

$$\theta_f = \frac{P}{1+C}\left[-\frac{1}{2}Y^2 + C_1 Y + C_2 - C_3 \cosh\left(\sqrt{\frac{D(1+C)}{C}}Y\right) - C_4\sinh\left(\sqrt{\frac{D(1+C)}{C}}Y\right) + C_5 \times\left\{\cosh\left(\sqrt{\frac{1}{Da}}Y\right) + \frac{1-\cosh\left(\sqrt{\frac{1}{Da}}\right)}{\sinh\left(\sqrt{\frac{1}{Da}}\right)}\sinh\left(\sqrt{\frac{1}{Da}}Y\right)\right\}\right] \tag{19}$$

$$\theta_s = P\left[Da\left\{\cosh\left(\sqrt{\frac{1}{Da}}Y\right) + \frac{1-\cosh\left(\sqrt{\frac{1}{Da}}\right)}{\sinh\left(\sqrt{\frac{1}{Da}}\right)}\sinh\left(\sqrt{\frac{1}{Da}}Y\right)\right\} - \frac{1}{2}Y^2 + C_1 Y - Da\right] - C\theta_f \tag{20}$$

where,

$$D_1 = D(1+C) - \frac{C}{Da}$$

$$N_1 = D(1+C)\sqrt{\frac{1}{Da}}\left\{1-\cosh\left(\sqrt{\frac{1}{Da}}\right)\right\}$$

$$N_2 = \frac{C}{Da}\sqrt{\frac{D(1+C)}{C}}\sinh\left(\sqrt{\frac{1}{Da}}\right)\sinh\left(\sqrt{\frac{D(1+C)}{C}}\right)$$

$$C_1 = 1 - \frac{\sqrt{Da}\left(\cosh\left(\sqrt{\frac{1}{Da}}\right) - 1\right)}{\sinh\left(\sqrt{\frac{1}{Da}}\right)}$$

$$C_2 = -Da + \frac{1}{D(1+C)}$$

$$C_3 = -\frac{C}{DaD(1+C)D_1}$$

$$C_4 = \frac{N_1 + N_2}{D(1+C)\sqrt{\frac{D(1+C)}{C}}\cosh\left(\sqrt{\frac{D(1+C)}{C}}\right)\sinh\left(\frac{\sqrt{1}}{Da}\right)D_1}$$

$$C_5 = Da - \frac{1}{D_1}$$

3.3. One-equation model

In the one-equation model, the governing equation can be obtained by assuming the temperatures of the fluid and solid phases are the same, i.e. $\theta_f = \theta_s = \theta$, and adding Eqs. (15) and (16). This leads to

$$(1+C)\frac{\partial^2\theta}{\partial Y^2} = U \tag{21}$$

where $\theta = \frac{\langle T\rangle - T_w}{q_w H/[(1-\varepsilon)k_s]}$ and $\langle T\rangle$ is a temperature averaged over the REV containing both the fluid and solid phases under the LTE assumption.

The pertinent boundary conditions are

$$\theta = 0 \quad \text{at } Y = 0 \tag{22}$$

$$\frac{\partial\theta}{\partial Y} = 0 \quad \text{at } Y = 1. \tag{23}$$

With the velocity distribution given by Eq. (7), the temperature profile can be readily obtained as

$$\theta = \frac{P}{1+C}\left[-\frac{1}{2}Y^2 + C_1 Y - Da\left\{1 - \cosh\left(\sqrt{\frac{1}{Da}}Y\right) - \frac{1-\cosh\left(\sqrt{\frac{1}{Da}}\right)}{\sinh\left(\sqrt{\frac{1}{Da}}\right)}\sinh\left(\sqrt{\frac{1}{Da}}Y\right)\right\}\right] \tag{24}$$

4. Temperature distributions and heat transfer characteristics

To validate the porous medium model of the microchannel heat sink and the analytical solutions based on that model, Eqs. (7), (19) and (20) are compared with the corresponding velocity and temperature distributions for the conjugate heat transfer problem comprising both the solid fin and the fluid. The formulation and the numerical method for the conjugate heat transfer problem are very similar to those in Sparrow et al. [14], and are not repeated here for brevity. Only the conventional energy equation is solved numerically, because a closed-form solution exists for the fully-developed channel flow in the form of [15]

$$U = \frac{\sum_{n=1,\,3,\ldots}^{\infty} -\frac{1}{n^4}\left[1 - \frac{\cosh\left(\frac{n\pi H}{w_c}(Y-0.5)\right)}{\cosh\left(\frac{n\pi H}{2w_c}\right)}\right]}{\sum_{n=1,\,3,\ldots}^{\infty} -\frac{1}{n^4}\left[1 - \frac{2w_c}{n\pi H}\tanh\left(\frac{n\pi H}{2w_c}\right)\right]} \tag{25}$$

Note that the velocity distribution given in Eq. (25) is the result of volume-averaging in the z-direction so that it may be compared with Eq. (7), which is the solution of the extended Darcy equation. In Fig. 2(a), for $Da = 10^{-3}$, Eq. (25) is compared with the analytical solution of the present study, Eq. (7). In Fig. 2(a), Eq. (7) is shown to predict the velocity profile of Eq. (25) within 1%. For the REV, the unidirectional flow in the x-direction can be modeled as the flow between two parallel plates. Hence, the permeability based on the Hagen–Poiseuille flow between two parallel plates is used in the present analysis, and this accounts for the microscopic viscous effect of side walls in the microchannel successfully.

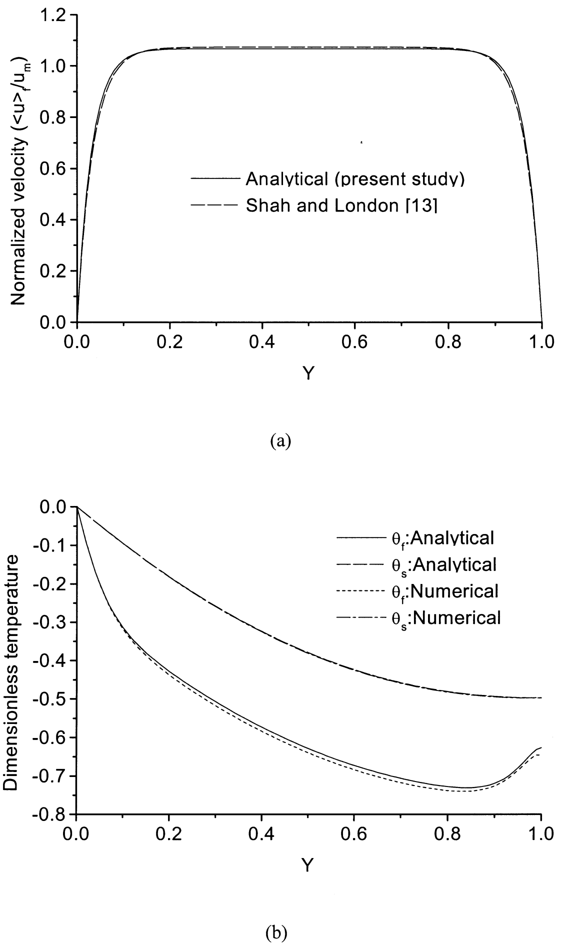

Fig. 2. Comparisons with solutions from conventional methods ($Da = 0.001$): (a) velocity; (b) temperature ($C = 0.005$).

Similarly, in Fig. 2(b), Eqs. (19) and (20) are compared with the corresponding volume-averaged temperature distributions from the numerical solutions. As mentioned before, numerical solutions for the fully-developed temperature distribution are obtained by using the finite difference method for the conjugate heat transfer problem composed of the fins and the microchannel between them. In Fig. 2(b), Eqs. (19) and (20) from the porous medium model are shown to be accurate in comparison with these numerical solutions up to 3%. This excellent agreement is mainly due to the appropriate local heat transfer coefficient for the fully-developed flow in the microchannel h_l, which is obtained from the numerical solution for the fully-developed flow in the microchannel. This accounts for the interfacial thermal interaction between the fins and the fluid flowing in the microchannel. It goes without saying that these analytical solutions from the porous medium model are helpful in identifying and studying the effects of variables of engineering importance. So the extension to more practical research, such as optimization of the microchannel heat sink, is possible without tedious numerical computations, which is illustrated in [5].

The analytical solutions Eqs. (19) and (20) show that the dimensionless temperatures, θ_f and θ_s, are functions of Da, C and D, Note that the equivalent Biot number D depends on the Darcy number Da and the effective conductivity ratio C, since, by using Eq. (4), D can be expressed as

$$D = \frac{H^2}{(1-\varepsilon)k_s} h_l a = CNu_{\infty,l}\left(\frac{1}{12Da} + \frac{1}{\sqrt{12Da}}\right) \qquad (26)$$

where $Nu_{\infty,l} = \frac{h_l d_h}{k_f}$ and d_h is hydraulic diameter of the microchannel. Hence, θ_f, θ_s, and θ (from Eq. (24)) are functions of Da and C. The temperature distributions for the fluid and solid phases obtained from the two-equation model θ_f and θ_s, are depicted together with the temperature profiles from the one-equation model, θ, in Figs. 3 and 4 for a range of parameters, Da and C. In these figures, the values of the key parameters, Da and C, are chosen so that the influence of each parameter on the temperature profiles can be clearly illustrated.

As shown in Figs. 3 and 4, the temperature difference between the two phases decreases as either Da decreases or C increases. In Figs. 3(c) or 4(c), the fluid temperature is not distinguishable from the solid temperature for $Da = 0.001$ and $C = 1.0$, in which case the LTE can be assumed and the one-equation model would be appropriate. As Da decreases (or as α_s increases) while C and the channel height H are fixed, the channel width w_c decreases. The channel height (a length scale used for non-dimensionalization) is arbitrarily fixed to help in better explaining the effect of Da on the temperature distributions illustrated in Fig. 3. The decrease in w_c in turn results in the increase in the interstitial heat transfer coefficient as well as the increase in the specific wetted area available for the heat transfer between the solid and the fluid. Both of these are responsible for the decrease in the temperature difference between the phases. On the other hand, the temperature difference between the phases decreases as C increases. The effective thermal conductivity ratio, C represents the ratio of the heat conductance between the fluid and the solid [11]. Thus the increase in C can be interpreted as the relative increase in the heat conductance through the fluid phase compared to that through the solid phase. Therefore, as C increases, the heat supplied from the bottom surface tends to be transferred directly to the fluid rather than detouring through the solid and finally to the fluid. This implies the decrease in the amount of heat transfer between the phases, where in turn results in the

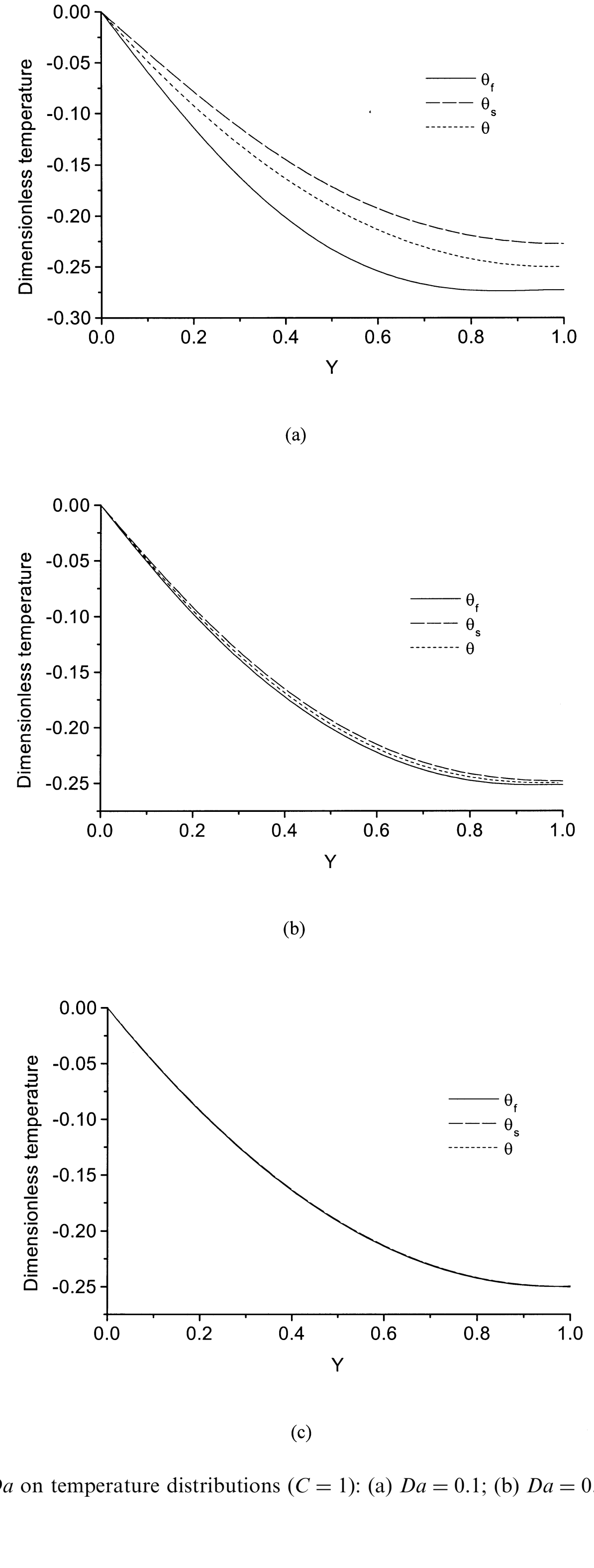

Fig. 3. Effect of Da on temperature distributions ($C = 1$): (a) $Da = 0.1$; (b) $Da = 0.01$; (c) $Da = 0.001$.

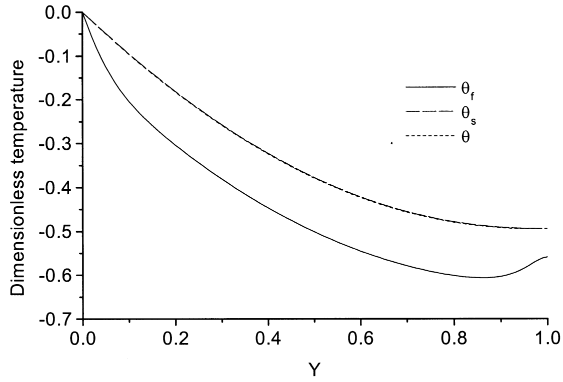

(a)

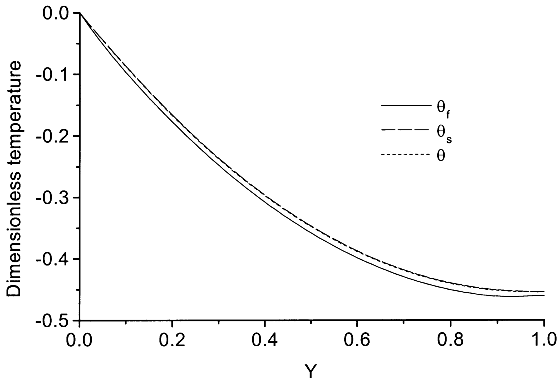

(b)

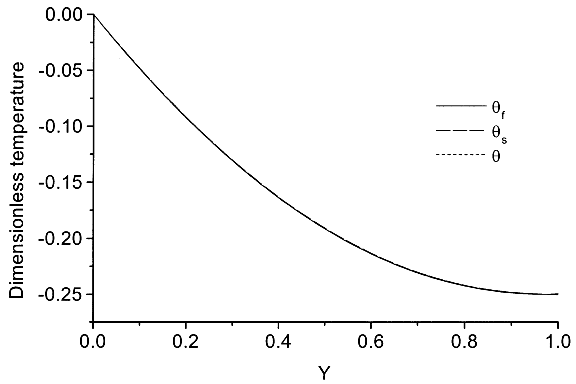

(c)

Fig. 4. Effect of C on temperature distributions ($Da = 0.001$): (a) $C = 0.01$; (b) $C = 0.1$; (c) $C = 1$.

decrease in the temperature difference between the phases.

It is important in thermal management of the electronic equipment to enhance the heat transfer rate between the heated wall and the fluid, i.e., the convection heat transfer rate in the heat sink. As a measure of the convection heat transfer rate, the overall Nusselt number is typically used. From the analytical solutions for the velocity and fluid temperature distributions, the overall Nusselt number of the microchannel heat sink can be determined as

$$Nu_{\infty,\,\mathrm{o}} = \frac{2Hh_\mathrm{m}}{\varepsilon k_\mathrm{f}} = \frac{2q_\mathrm{w}H}{\varepsilon k_\mathrm{f}(T_\mathrm{w}-T_\mathrm{b})} = -\frac{2}{C\int_0^1 U\theta_\mathrm{f}\,\mathrm{d}Y} = -\frac{2}{C\theta_{\mathrm{f,\,b}}}, \tag{27}$$

where T_b and h_m are the bulk-mean temperature of the fluid and the heat transfer coefficient between the heat sink base and the fluid based on the bulk-mean temperature, respectively. After some manipulation using Eqs. (7) and (19), the dimensionless bulk-mean temperature for the microchannel heat sink can be obtained in a closed-form as the one shown in Appendix A. Since U is a function of Da, and θ_f is a function of Da and C, $Nu_{\infty,\,\mathrm{o}}$ is also a function of Da and C.

Now, several limiting behaviors of heat transfer characteristics in the microchannel heat sink are studied by examining limiting values of $Nu_{\infty,\,\mathrm{o}}$. As Da approaches infinity (or $\alpha_\mathrm{s}\rightarrow 0$), it can be easily seen from Eq. (27) that

$$\lim_{Da\rightarrow\infty} Nu_{\infty,\,\mathrm{o}} = 5.385, \tag{28}$$

which is identical to the Nusselt number for fully-developed convective flow between parallel plates with uniform heat flux on one side and insulated on the other side. [13] This is because, as Da approaches infinity, the heat and fluid flow characteristics of the microchannel heat sink approach those of convective flow between parallel plates where top plate is insulated and bottom plate is uniformly heated, and $\varepsilon = 1$ for this case. On the other hand, as Da approaches 0, it can be also shown from Eq. (27),

$$\lim_{Da\rightarrow 0} Nu_{\infty,\,\mathrm{o}} = \frac{6(1+C)}{C} \tag{29}$$

In this case, the boundary effect of top and bottom surfaces is negligible and the heat transfer area between the fin and the fluid is so large that the temperature difference between the fluid and solid phases is negligible. Hence, it is not surprising to see that the Nusselt number matches with Eq. (29) when the flow is assumed to be Darcian and the fluid in LTE with the solid. This agreement in the overall Nusselt numbers shows that the porous medium approach can predict the thermal performance of the microchannel heat sink accurately for broad range of parameters.

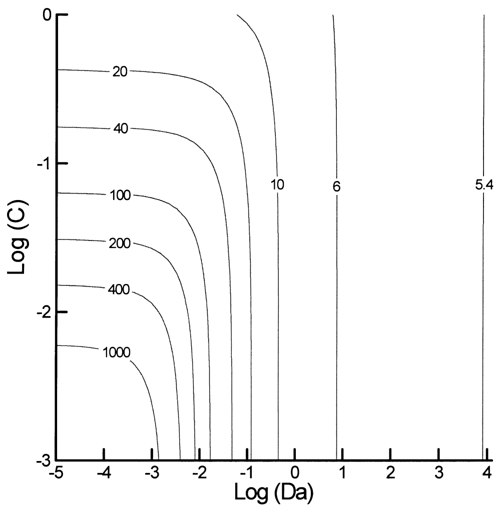

Fig. 5. Contour map of the overall Nusselt number, $Nu_{\infty,\,\mathrm{o}}$.

In order to show influences of Da and C on the thermal performance of the microchannel heat sink more clearly, the contour map of the overall Nusselt number with respect to Da and C, is presented in Fig. 5. In this figure, $Nu_{\infty,\,\mathrm{o}}$ increases as either Da or C decreases, which is resulted from the increase in the local heat transfer coefficient or the decrease in the thermal resistance through the fin. More importantly, $Nu_{\infty,\,\mathrm{o}}$ is shown in Fig. 5 to approach an asymptotic value as either Da decreases while C is held constant or C decreases while Da is held constant. The former is because the heat sink fins lose their efficiency as their length increases over a certain value, and the latter is because the ratio of the conduction resistance through the fins to the convection resistance gets smaller. This implies there is a practical limit in the values of the Darcy number and the effective thermal conductivity ratio below which the heat transfer performance of the microchannel heat sink would not be increased further. For example, in the case of $C = 0.0631$ ($\mathrm{Log}(C) = -1.2$), increase in the overall Nusselt number is shown to be negligible for $Da \leq 0.000316$ ($\mathrm{Log}(Da) \leq -3.5$) which is a practical limit in this case.

5. Discussion on the applicability of the local thermal equilibrium assumption

In the previous section, the temperature profiles from the two-equation model and the one-equation model are compared and the qualitative discussion on the LTE is presented. In the present section, the applicability of the LTE and the corresponding one-equation model is analyzed quantitatively and the asymptotic behavior of the temperature difference between the phases is examined.

To validate the LTE assumption, the local temperature difference between the fluid and solid phases should be negligibly small. Hence, we can define E_{LTE} as a measure of the validity of the LTE as follows;

$$E_{\mathrm{LTE}} \equiv \frac{\theta_{\mathrm{f}} - \theta_{\mathrm{s}}}{\theta} \ll 1 \tag{30}$$

This definition is similar to the one used by Quintard and Whitaker [16] for the transient conduction problem in the porous medium. In the above definition, the temperature obtained from the one-equation model is used as a scale temperature for the temperature difference between the phases. Here, θ means the difference between the volume-averaged temperature of the heat sink (for the representative element volume containing both the fluid and solid phases) and the heated wall temperature under the LTE assumption. Even though it is certain that Eq. (30) validates the application of the one-equation model, another figure of merit, E_{1EQ} is introduced to check more directly the validity of using the one-equation model as follows;

$$E_{\mathrm{1EQ}} \equiv \frac{\theta_{\mathrm{f}} - \theta}{\theta_{\mathrm{f}}} \ll 1 \tag{31}$$

In the above definition, the relative error E_{1EQ} is defined as the relative error for estimating the fluid temperature using the one-equation model. The reason for choosing the fluid temperature instead of the solid temperature in the above definition is because the fluid temperature obtained from the two-equation model is shown in Fig. 4 to be farther away from the temperature obtained using the one-equation model. Hence the above definition based on the fluid temperature would be more stringent than the one based on the solid temperature.

The order of magnitude analysis is helpful in estimating the asymptotic behavior of E_{LTE} for the limiting cases where Da becomes infinitesimally small or C becomes infinitely large. From Eqs. (15), (16) and (21), a differential equation comprising both $\theta_{\mathrm{f}} - \theta_{\mathrm{s}}$ and θ can be obtained as

$$C\frac{\mathrm{d}^2(\theta_{\mathrm{f}} - \theta_{\mathrm{s}})}{\mathrm{d}Y^2} - D(1+C)(\theta_{\mathrm{f}} - \theta_{\mathrm{s}}) = (1+C)\frac{\mathrm{d}^2\theta}{\mathrm{d}Y^2} \tag{32}$$

The magnitude of E_{LTE} can be estimated from Eq. (32) as

$$\frac{(\theta_{\mathrm{f}} - \theta_{\mathrm{s}})}{\theta} = O\left(\frac{1+C}{C + D(1+C)}\right) \tag{33}$$

Then, the asymptotic behavior of E_{LTE} can be easily estimated by using Eq. (33) as

$$\frac{(\theta_{\mathrm{f}} - \theta_{\mathrm{s}})}{\theta} = \begin{cases} O\left(\dfrac{12Da}{CNu_{\infty,1}}\right) & \text{when } Da \ll 1 \\ O\left(\dfrac{12Da}{CNu_{\infty,1}\left(\sqrt{12Da}+1\right)}\right) & \text{when } C \gg 1 \end{cases} \tag{34}$$

Eq. (34) shows that Da and C simultaneously affect the magnitude of E_{LTE} and confirms the tendency that the difference between θ_{f} and θ_{s} decreases as either Da decreases or C increases, as discussed in Section 4. In porous media, C is usually smaller than 1 and Da is much smaller than 1. Hence, the first equation in Eq. (34) is practically more useful in validating the LTE assumption and the corresponding one-equation model. The first equation in Eq. (34) can be simplified further by considering that $Nu_{\infty,1}$ converges to a constant value, 10.4, as Da decreases when the laminar flow dominates within the porous medium [5]. From the order of magnitude analysis, the first equation in Eq. (34) can be rewritten as

$$E_{\mathrm{LTE}} = O\left(\frac{Da}{C}\right) \quad \text{when } Da \ll 1 \tag{35}$$

Eq. (35) shows that E_{LTE} is simply represented by Da/C. As mentioned above, laminar flow is assumed in derivation of Eq. (35). In case of turbulent flow, the Nusselt number in the pore level, $Nu_{\infty,1}$ increases with the increase in the fluid velocity due to the dispersion effect [10]. In this case, E_{LTE} becomes even smaller than $O(Da/C)$ since the thermal communication between the phases gets more effective which results in the decrease in the temperature difference. Consequently, E_{LTE} can not be larger than $O(Da/C)$ and Eq. (35) would be considered as a conservative estimate when validating the LTE assumption.

Since $0 > \theta_{\mathrm{s}} > \theta > \theta_{\mathrm{f}}$, from the definitions of E_{LTE} and E_{1EQ}, we can infer that $E_{\mathrm{LTE}} > E_{\mathrm{1EQ}}$ which implies that the condition for LTE to be valid is a sufficient condition for the one-equation model to be valid. Hence, we can safely assume that E_{1EQ} would exhibit the same asymptotic behavior as E_{LTE} in the limiting cases where either Da approaches a very small value or C approaches a very large value.

As pointed out in Section 4, θ_{f} and θ are functions of Da and C. Hence, E_{1EQ} is a function of Da and C. Fig. 6 shows the contour map of averaged in the y-direction by using the analytical solutions, Eqs. (19) and (24). In this figure, E_{1EQ} is shown to decrease as

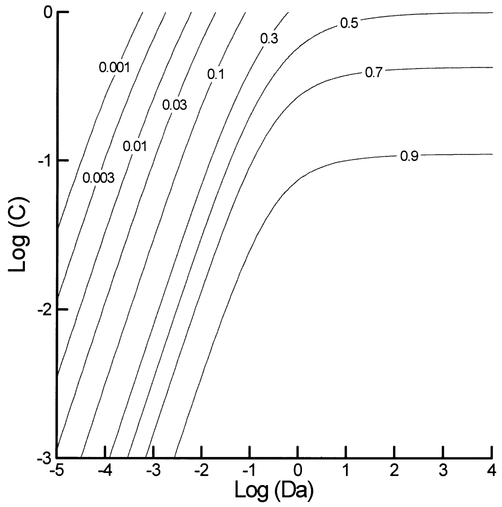

Fig. 6. Contour map of E_{1EQ}.

either Da decreases or C increases, and this confirms the qualitative discussion in Section 4. From this tendency, Fig. 6 can be practically applied to the microchannel heat sink in checking if it is valid to use the one-equation model for thermal analysis of the microchannel heat sink. For example, in the region above the contour line of $E_{1EQ} = 0.1$, we can expect the relative error for using the one-equation model to be smaller than 0.1.

It is in order to check if the one-equation model is valid in practical microchannel heat sinks. As a material of heat sink, we typically use silicon, aluminum or copper. If we choose water as a coolant and set the practical limit of Da to 0.000833 (or $\alpha_s = 10$) by accounting for the manufacturing capability and the cost for machining the microchannel, the values of E_{1EQ} can be obtained from Fig. 6 for various porosities and solid materials. The results are summarized in Table 1. From Table 1, it can be shown that the one-equation model can be practically applied to microchannel heat sinks only when the heat sink is highly porous. With a practically allowable relative error E_{1EQ} of 0.1, the recommended porosity for the one-equation model to be valid is larger than 0.9. If air is used instead as a coolant, the values of C are much less than those for the case of water and the recommended porosity is expected to be very close to 1.

6. Conclusion

In this paper, direct descriptions on the relation between the microstructure of the porous medium and the macroscopic convective heat transfer in the porous medium are presented for a well-defined porous medium, the microchannel heat sink. The applicability of the one-equation model for the microchannel heat sink when the microchannel heat sink is treated as a porous medium is also presented. Analytical solutions for temperature distribution are obtained by using both the one-equation and two-equation models for the case where the bottom surface is uniformly heated and the top surface is insulated. Variables of engineering importance are identified as Darcy number Da and effective thermal conductivity ratio C from the analytical solutions, and their effects on the heat transfer in the microchannel heat sink are studied. As either Da decreases or C increases, the fluid temperature approaches the solid temperature, in which case the LTE assumption and the one-equation model would be appropriate. In addition, as either one of Da and C decreases, the overall Nusselt number of the microchannel heat sink $Nu_{\infty,o}$ is shown to increase to an asymptotic value. To check the validity of the LTE assumption and the corresponding one-equation model, the relative temperature difference between the phases E_{LTE} and the relative error for using the one-equation model E_{1EQ} are defined. The asymptotic behavior of E_{LTE} is examined by using the order of magnitude analysis to present the overall tendency in relation to the validity of the LTE assumption and the

Table 1
E_{1EQ} in practical microchannel heat sinks ($\alpha_s = 10, Da = 0.0008333$)

ε	Silicon and water		Aluminium and water		Copper and water	
	C	E_{1EQ}	C	E_{1EQ}	C	E_{1EQ}
0.50	0.00413	0.407	0.00258	0.524	0.00152	0.652
0.60	0.00620	0.314	0.00387	0.423	0.00228	0.555
0.70	0.00964	0.226	0.00602	0.320	0.00355	0.444
0.80	0.0165	0.145	0.0103	0.215	0.00608	0.318
0.90	0.0372	0.069	0.0232	0.107	0.0137	0.170
0.99	0.409	0.005	0.255	0.009	0.150	0.016

one-equation model. The asymptotic behavior is shown to be on the order of Da/C, which confirms the tendency that the temperature difference between θ_f and θ_s decreases as either Da decreases or C increases. Since $0 > \theta_s > \theta > \theta_f$, it can be inferred that $E_{LTE} > E_{1EQ}$ which implies that the condition for LTE to be valid is a sufficient condition for the one-equation model to be valid. Finally, the relative error map in terms of Da and C is presented to identify the applicable region of the one-equation model in practical problems involving the microchannel heat sinks. In conclusion, the one-equation model can be practically applied to microchannel heat sinks only with very high porosity.

Acknowledgements

This work was supported by EPRC (Electronic Packaging Research Center) at KAIST, and MOST (Ministry of Science and Technology).

Appendix

$$
\begin{aligned}
\theta_{f,\,b} = \frac{P^2}{1+C}\Bigg[\Bigg\{ & 2Da^{3/2} + \left(\frac{5}{2} - C_1 - 2C_2 - \frac{5}{4}C_5\right)\sqrt{Da} + C_3\frac{\sqrt{\frac{1}{Da}}}{\frac{1}{Da} - \frac{D(1+C)}{C}}\Bigg\}\frac{1-\cosh\left(\sqrt{\frac{1}{Da}}\right)}{\sinh\left(\sqrt{\frac{1}{Da}}\right)} \\
& - \frac{C_3}{2}\frac{1}{\sqrt{\frac{1}{Da}} + \sqrt{\frac{D(1+C)}{C}}}\sinh\left(\sqrt{\frac{1}{Da}} + \sqrt{\frac{D(1+C)}{C}}\right) - \frac{C_3}{2}\frac{1}{\sqrt{\frac{1}{Da}} - \sqrt{\frac{D(1+C)}{C}}}\sinh\left(\sqrt{\frac{1}{Da}} - \sqrt{\frac{D(1+C)}{C}}\right) \\
& - \frac{C_3}{2}\frac{1}{\sqrt{\frac{1}{Da}} + \sqrt{\frac{D(1+C)}{C}}}\frac{\cosh\left(\sqrt{\frac{1}{Da}} + \sqrt{\frac{D(1+C)}{C}}\right)}{\sinh\left(\sqrt{\frac{1}{Da}}\right)} + \frac{C_3}{2}\frac{\sqrt{\frac{1}{Da}}}{\frac{1}{Da} - \frac{D(1+C)}{C}}\frac{\cosh\left(2\sqrt{\frac{1}{Da}} + \sqrt{\frac{D(1+C)}{C}}\right)}{\sinh\left(\sqrt{\frac{1}{Da}}\right)} \\
& + \frac{C_3}{2}\frac{\sqrt{\frac{1}{Da}}}{\frac{1}{Da} - \frac{D(1+C)}{C}}\frac{\cosh\left(\frac{\sqrt{D(1+C)}}{C}\right)}{\sinh\left(\sqrt{\frac{1}{Da}}\right)} - \frac{C_3}{2}\frac{1}{\sqrt{\frac{1}{Da}} - \sqrt{\frac{D(1+C)}{C}}}\frac{\cosh\left(\sqrt{\frac{1}{Da}} - \sqrt{\frac{D(1+C)}{C}}\right)}{\sinh\left(\sqrt{\frac{1}{Da}}\right)} \\
& + C_3\sqrt{\frac{C}{D(1+C)}}\sinh\left(\sqrt{\frac{D(1+C)}{C}}\right) - \frac{C_4}{2}\frac{1}{\sqrt{\frac{1}{Da}} + \sqrt{\frac{D(1+C)}{C}}}\cosh\left(\sqrt{\frac{1}{Da}} + \sqrt{\frac{D(1+C)}{C}}\right) \\
& + \frac{C_4}{2}\frac{1}{\sqrt{\frac{1}{Da}} - \sqrt{\frac{D(1+C)}{C}}}\cosh\left(\sqrt{\frac{1}{Da}} - \sqrt{\frac{D(1+C)}{C}}\right) - \frac{C_4}{2}\frac{1}{\sqrt{\frac{1}{Da}} + \sqrt{\frac{D(1+C)}{C}}}\frac{\sinh\left(\sqrt{\frac{1}{Da}} + \sqrt{\frac{D(1+C)}{C}}\right)}{\sinh\left(\sqrt{\frac{1}{Da}}\right)} \\
& + \frac{C_4}{4}\frac{1}{\sqrt{\frac{1}{Da}} + \sqrt{\frac{D(1+C)}{C}}}\frac{\sinh\left(2\sqrt{\frac{1}{Da}} + \sqrt{\frac{D(1+C)}{C}}\right)}{\sinh\left(\sqrt{\frac{1}{Da}}\right)} + \frac{C_4}{2}\frac{\sqrt{\frac{1}{Da}}}{\frac{1}{Da} - \frac{D(1+C)}{C}}\frac{\sinh\left(\sqrt{\frac{D(1+C)}{C}}\right)}{\sinh\left(\sqrt{\frac{1}{Da}}\right)} \\
& + \frac{C_4}{2}\frac{1}{\sqrt{\frac{1}{Da}} - \sqrt{\frac{D(1+C)}{C}}}\frac{\sinh\left(\sqrt{\frac{1}{Da}} - \sqrt{\frac{D(1+C)}{C}}\right)}{\sinh\left(\sqrt{\frac{1}{Da}}\right)} - \frac{C_4}{4}\frac{1}{\sqrt{\frac{1}{Da}} - \sqrt{\frac{D(1+C)}{C}}}\frac{\sinh\left(2\sqrt{\frac{1}{Da}} - \sqrt{\frac{D(1+C)}{C}}\right)}{\sinh\left(\sqrt{\frac{1}{Da}}\right)}
\end{aligned}
$$

$$+C_4\sqrt{\frac{C}{D(1+C)}}\cosh\left(\sqrt{\frac{D(1+C)}{C}}\right)+\frac{C_5}{2}\sqrt{Da}\sinh\left(2\sqrt{\frac{1}{Da}}\right)+(1-C_5)\sqrt{Da}\sinh\left(\sqrt{\frac{1}{Da}}\right)+\frac{C_5}{4}\sqrt{Da}\frac{1-\cosh\left(3\sqrt{\frac{1}{Da}}\right)}{\sinh\left(\sqrt{\frac{1}{Da}}\right)}$$

$$-2C_5\frac{1-\cosh\left(\sqrt{\frac{1}{Da}}\right)}{\sinh^2\left(\sqrt{\frac{1}{Da}}\right)}+Da+\frac{1}{6}-\frac{1}{2}C_1-C_2-C_4\left(\frac{\sqrt{\frac{D(1+C)}{C}}}{\frac{1}{Da}-\frac{D(1+C)}{C}}+\sqrt{\frac{C}{D(1+C)}}\right)-\frac{C_5}{2}\Bigg]$$

References

[1] D.B. Tuckerman, R.F.W. Pease, High-performance heat sinking for VLSI, IEEE Electron Device Letter 2 (1981) 126–129.

[2] D.B. Tuckerman, R.F.W. Pease, Ultrahigh thermal conductance microstructures for integrated circuits, in: IEEE Proc. 32nd Electronics Conference, 1982, pp. 145–149.

[3] J.C.Y. Koh, R. Colony, Heat transfer of microstructures for integrated circuits, Int. Comm. Heat Mass Transfer 13 (1986) 89–98.

[4] C.L. Tien, S.M. Kuo, Analysis of forced convection in microstructures for electronic system cooling, in: Proc. Int. Symp. Cooling Technology for Electronic Equipment, Honolulu, HI, 1987, pp. 217–226.

[5] S.J. Kim, D. Kim, Forced convection in microstructures for electronic equipment cooling, ASME J. Heat Transfer 121 (1999) 635–645.

[6] M. Kaviany, Laminar flow through a porous channel bounded by isothermal parallel plates, Int. J. Heat Mass Transfer 28 (1985) 851–858.

[7] K. Vafai, S.J. Kim, Forced convection in a channel filled with a porous medium: an exact solution, ASME J. Heat Transfer 111 (1989) 1103–1106.

[8] D. Poulikakos, K. Renken, Forced convection in a channel filled with porous medium, including the effects of flow inertia, variable porosity, and Brinkman friction, ASME J. Heat Transfer 109 (1987) 880–888.

[9] R.G. Carbonell, S. Whitaker, Heat and mass transfer in porous media, in J. Bear and M.Y. Corapcioglu (Eds.), Fundamentals of Transport Phenomena in Porous Media, Martinus Nijhoff, Dordrecht, 1984, pp. 121–198.

[10] A. Amiri, K. Vafai, Analysis of dispersion effects and non-thermal equilibrium, non-Darcian, variable porosity incompressible flow through porous media, Int. J. Heat Mass Transfer 37 (1994) 939–954.

[11] D.Y. Lee, K. Vafai, Analytical characterization and conceptual assessment of solid and fluid temperature differentials in porous media, Int. J. Heat Mass Transfer 42 (1999) 423–435.

[12] K. Vafai, C.L. Tien, Boundary and inertia effects on flow and heat transfer in porous media, Int. J. Heat Mass Transfer 24 (1981) 195–203.

[13] A. Bejan, Convection Heat Transfer, 2nd ed., Wiley, New York, 1995 (Chapter 12).

[14] E.M. Sparrow, B.R. Baliga, S.V. Patankar, Forced convection heat transfer from a shrouded fin array with and without tip clearance, ASME Journal of Heat Transfer 100 (1978) 572–579.

[15] R.K. Shah, A.L. London, Laminar Flow Forced Convection in Ducts, Academic Press, New York, 1978 (Chapter 7).

[16] M. Quintard, S. Whitaker, Local thermal equilibrium for transient heat conduction: theory and comparison with numerical experiments, Int. J. Heat Mass Transfer 38 (1995) 2779–2796.